Materials Horizons

ROYAL SOCIETY OF CHEMISTRY

COMMUNICATION

View Article Online
View Journal

Cite this: DOI: 10.1039/d6mh00635c

Received 1st April 2026,
Accepted 21st April 2026

DOI: 10.1039/d6mh00635c

rsc.li/materials-horizons

A triply periodic minimal surface-based acoustic crystal with double-zero index

Yafeng Chen, †*[a] Shanjun Liang,†[b] Zhihao Lan,[cf] Zhongming Gu,[a] Zhongqing Su*[d] and Jie Zhu*[ae]

Three-dimensional (3D) acoustic crystals (ACs) with a double-zero index exhibit unique properties akin to a 3D void space, enabling transformative applications in acoustic wave cloaking, tunneling, and wavefront shaping. However, existing 3D ACs with a double-zero index are all made of disconnected solid structures, posing significant fabrication challenges for diverse applications. Here, we propose a fabrication-friendly triply periodic minimal surface (TPMS)-based AC with a double-zero index, resulting from a Dirac-like cone accidentally degenerated by three dipolar modes and one monopolar mode. The exotic functionalities of acoustic wave tunneling and cloaking characterized by the double-zero index are experimentally demonstrated. Meanwhile, the tunable mechanical properties of the TPMS-based AC are exhibited. The developed TPMS-based AC overcomes the fabrication limitations of conventional 3D double-zero-index acoustic structures while providing superior mechanical performance, paving the way for the development of multifunctional acoustic devices.

New concepts

This paper proposes a fabrication-friendly triply periodic minimal surface-based acoustic crystal with a double-zero index. Three-dimensional (3D) acoustic crystals (ACs) with a double-zero index exhibit unique properties akin to a 3D void space, enabling transformative applications in acoustic wave cloaking, tunneling, and wavefront shaping. However, existing 3D ACs with a double-zero index are all made of disconnected solid structures, posing significant fabrication challenges for diverse applications. Meanwhile, triply periodic minimal surfaces (TPMSs) featuring superior mechanical properties provide a route for the development of lightweight and multifunctional devices. To date, TPMSs have been integrated with acoustic metamaterials for insulating acoustic/elastic waves and the robust manipulation of acoustic and elastic waves, and possess both superior mechanical and acoustic properties. However, realizing double-zero acoustic index in a TPMS is still unexplored. This paper achieved breakthroughs in the following aspects: (a) A fabrication-friendly TPMS-based AC with a double-zero index is developed and the exotic functionalities of acoustic wave tunneling and cloaking characterized by the double-zero index are experimentally demonstrated. (b) The tunable mechanical properties of the TPMS-based AC are exhibited. The developed TPMS-based AC overcomes the fabrication limitations of conventional 3D double-zero-index acoustic structures while providing superior mechanical performance, paving the way for the development of multifunctional acoustic devices.

1. Introduction

Triply periodic minimal surfaces (TPMSs) are a class of periodic structures in differential geometries that exhibit minimal surface properties, characterized by zero mean curvature, providing an efficient tessellation of space.[1] Due to their unique geometric properties, these shell-based structures possess ultrahigh strength-to-weight ratios and reduced sensitivity to stress concentrations compared to truss-based cellular materials. To date, TPMS have exhibited exceptional functionalities, such as energy absorption, fracture resistance, thermal management, and biomimetic designs.[2–12] These unique properties make TPMS highly appealing for a wide range of applications, spanning aerospace, civil, mechanical, and biomedical engineering.

Beyond the study of mechanical properties in advanced materials and structures, explorations into the acoustic properties of artificial structures have also attracted considerable attention.[12–15] Recently, leveraging periodic minimal surfaces to control acoustic/elastic waves, that is integrating acoustic

[a] Institute of Acoustics, School of Physics Science and Engineering, Tongji University, 200092, Shanghai, China. E-mail: yachen@tongji.edu.cn, jiezhu@tongji.edu.cn
[b] Division of Science, Engineering and Health Studies, College of Professional and Continuing Education, Hong Kong Polytechnic University, Hong Kong SAR, China
[c] Department of Electronic and Electrical Engineering, University College London, London WC1E 7JE, UK
[d] Department of Mechanical Engineering, The Hong Kong Polytechnic University, Kowloon, Hong Kong SAR, China. E-mail: zhongqing.su@polyu.edu.hk
[e] Shanghai Research Institute for Intelligent Autonomous Systems, Tongji University, Shanghai 201210, China
[f] College of Physical Sciences and Engineering, Mohammed VI Polytechnic University, 43150, Ben Guerir, Morocco
† These authors contribute equally to this work.

metamaterials[16–18] with TPMS to design lightweight and multifunctional devices, has attracted great attention. Examples include creating TPMSs with acoustic/elastic bandgaps for insulating acoustic/elastic waves,[6] constructing Helmholtz cavities within TPMSs for simultaneous superior acoustic and mechanical energy absorptions,[19] and engineering topological states within TPMSs for the robust manipulation of acoustic and elastic waves.[2,5] Despite these advancements on leveraging TPMSs to achieve concurrent acoustic and mechanical functionalities, engineering TPMSs with acoustic double-zero-index, an important acoustic property, remains unexplored. The double-zero-index medium was originally discovered in photonic crystals with a Dirac-like cone.[20–22] At the frequency of the Dirac-like point, the effective permittivity and permeability both equal zero.[23–30] Hence, such a medium can be used as an electromagnetic void space, where electromagnetic waves do not experience any phase accumulation.[31–33] Thereafter, by engineering a Dirac-like cone in acoustic crystals (ACs), double-zero-index acoustic metamaterials were developed.[34,35] Dubois *et al.* developed a two-dimensional AC with a Dirac-like cone degenerated by high-order monopolar and dipolar modes, at the frequency of which the effective density and reciprocal of bulk modulus simultaneously equal zero.[35] As there is no phase accumulation for acoustic waves propagating in a double-zero-index acoustic medium, exotic functionalities, such as wavefront shaping, cloaking, focusing and tunneling of acoustic waves, can be achieved. Xu *et al.* further designed a three-dimensional (3D) glide-symmetric AC with a four-fold degenerate Dirac-like point, achieving the acoustic double-zero-index in 3D space.[36] Very recently, a phononic Weyl semimetal with deterministic double-zero index was developed.[37] However, in the unit cell of these structures, the scatters are disconnected within the 3D space; thus, it is needed to introduce extra support structures to connect these structures. This makes fabrication challenging for diverse application scenarios where the unit cells need to be arranged into a specific configuration to achieve the specific functions, such as cloaking, focusing and so on.

Given the important application potential of double-zero-index media, it is highly desirable to create a fabrication-friendly structure with this property for diverse and large-scale practical applications.

Here, we design a 3D TPMS-based AC that hosts a Dirac-like cone accidentally degenerated by three dipolar modes and one monopolar mode. At the frequency of the Dirac-like point, the effective mass density and the reciprocal of the bulk modulus simultaneously equal zero. By fabricating the structure *via* 3D printing, we experimentally demonstrate exotic functionalities of acoustic wave tunneling and cloaking. The utilization of a TPMS not only overcomes the current fabrication challenge of 3D double-zero-index AC but also endows the structure with lightweight and superior mechanical properties, making it favorable for the development of multifunctional integrated acoustic devices.

2. Results

Here, we select the Schoen-I-graph and wrapped package (IWP)-type TPMS to construct the scatter of the AC, governed by the following level-set equation:

$$\begin{aligned} f(x,y,z) = {} & 2\left(\cos\left(\frac{2\pi x}{a}\right)\times\cos\left(\frac{2\pi y}{a}\right)+\cos\left(\frac{2\pi y}{a}\right)\right. \\ & \left.\times\cos\left(\frac{2\pi z}{a}\right)+\cos\left(\frac{2\pi x}{a}\right)\times\cos\left(\frac{2\pi z}{a}\right)\right) \\ & -\left(\cos\left(\frac{2x}{a}\right)+\cos\left(\frac{2y}{a}\right)+\cos\left(\frac{2z}{a}\right)\right) \end{aligned} \quad (1)$$

where a = 5 cm denotes the lattice constant. We use the TPMS Designer[38] by setting the Isovalue v1 as 0.36 [see Section S1 of the SI for details], with the volume fraction of 0.335, to generate the geometry of the TPMS, which acts as the scatter, as shown in Fig. 1a (denoted by the TPMS scatter). With the overall considerations of fabrication cost, air loss and test feasibility, the unit cell size is selected as 5 cm. We find that the scatter is connected into a bulk and, therefore, we can assemble it into any desirable structure that can be fabricated *via* 3D printing. As shown in Fig. 1b, the band diagram of the AC exhibits a four-fold degeneracy at the Γ point for the 2nd–5th bands at the frequency of 5.46 kHz. As illustrated in Fig. 1d, one monopolar mode and three dipolar modes are degenerated at this point. An enlarged view of the band diagram near the degenerate point in the k_x–k_y plane is plotted in Fig. 1c, showing a conical dispersion intersected by two flat bands. Meanwhile, in Section S1 of the SI, we also show that the dispersions in the k_x–k_z and k_y–k_z planes are the same as in Fig. 1c, meaning that conical dispersion appears in all directions in the vicinity of the four-fold degenerate point, a typical property of a Dirac-like cone in 3D space. The four-fold degenerate point is also called the Dirac-like point, which has been predicted to possess double-zero index.[36,37] To validate this, we extract the normalized effective mass density (ρ_{eff}) and the normalized effective compressibility (β_{eff}) using the method in ref. 36 as shown in Fig. 1e, from which one can observe that ρ_{eff} and β_{eff} both equal zero at the frequency of the Dirac-like point. Such a TPMS-based AC with a double-zero index can be used as a 3D acoustic void space for wave tunneling, cloaking and wavefront shaping. Meanwhile, we also experimentally measure the transmission ratio of the TPMS-based AC using the impedance tube, as shown in Fig. 1f, demonstrating that the transmission ratio maintains a relatively high value (higher that 0.75) over a frequency window of (5.2 kHz, 5.8 kHz), which is comparable with the measured transmission ratio of the two-dimensional double-zero index structure in ref. 35.

To experimentally validate the property of a 3D acoustic void space of the TPMS-based AC, we fabricated a structure consisting of 5 × 5 × 5 unit cells, as shown in Fig. 2a, and put it into a bent tube with hard boundaries. A schematic of the experimental setup is shown in Fig. 2b. As the simulation results show in Fig. 2c, the wave impinging normally to the TPMS-based AC along the negative z direction becomes positive in the

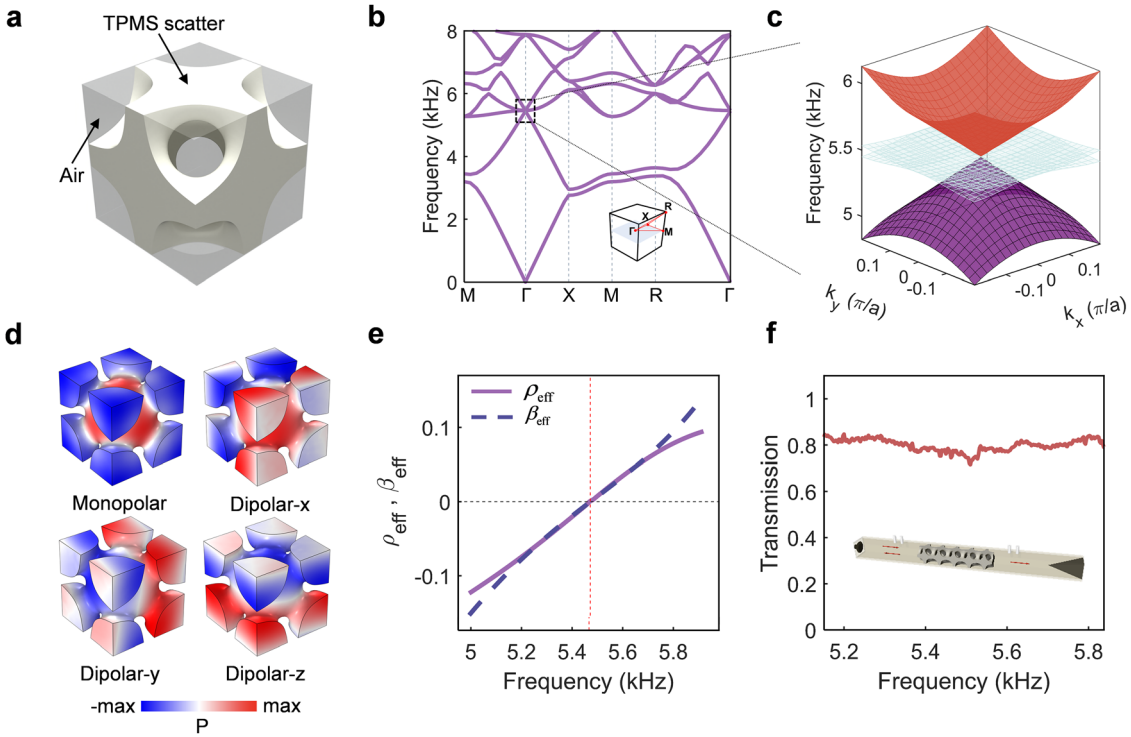

Fig. 1 The TPMS-based AC with a double-zero index. (a) The unit cell of the TPMS-based AC. (b) The band diagram of the TPMS-based AC with a four-fold degeneracy at the Γ point for the 2nd–5th bands. (c) The enlarged view of the band diagram near the degenerate point in the k_x–k_y plane. (d) The eigenmodes of one monopolar mode and three dipolar modes degenerated at the Dirac-like point. (e) The extracted normalized effective mass density (ρ_{eff}) and normalized effective compressibility (β_{eff}). (f) The measured transmission ratio of the TPMS-based AC using the impedance tube.

x direction, with a 90° bend, without distortion. Meanwhile, we have also provided the simulation with thermoviscous boundary layer effects in the SI (Section S3), indicating that the effects of thermal and viscous losses are negligible herein. Fig. 2d demonstrates the experimentally measured field (the test domain is denoted by the dashed box in Fig. 2c), which agrees well with the simulation result. Fig. 2e shows the fast Fourier transform (FFT) of the acoustic pressure fields measured within the horizontal (upper panel) and vertical (bottom panel) planes. One can observe that, at the frequency of the Dirac-like point (5.46 kHz), there is a peak of FFT amplitude at $k_y = 0$ (upper panel) and $k_z = 0$ (bottom panel), implying that the wave vector of the acoustic wave exiting from the TPMS-based AC is only dominated by k_x. This indicates that the acoustic wave maintains a planar wave front even when it experiences a 90° bend. However, when the frequencies are above and below the frequency of the Dirac-like point, the exiting waves possess non-zero k_y and k_z components that expand into a circle, meaning that the planar acoustic wave is distorted.

Next, we further experimentally demonstrate that the TPMS-based AC with a double-zero index can be used for cloaking. As sketched in Fig. 3a, we introduce an obstacle into the structure (consisting of 8 × 8 × 3 unit cells) by removing 2 × 2 × 3 unit cells and using the hard boundaries to replace them. The experimental schematic is shown in Fig. 3b. Fig. 3c demonstrates the simulated acoustic pressure field at the frequency of the Dirac-like point, from which we can find that the output wave still maintains the planar wave front even when an obstacle is introduced. Fig. 3d shows the measured acoustic pressure fields, which match well with the simulated result. As a comparison, we remove the TPMS-based AC and keep the obstacle, and the measured field in this condition shown in Fig. 3e demonstrates that the acoustic wave is distorted, illustrating the function of the TPMS-based AC to keep the planar wavefront of the output acoustic waves.

It is well-known that TPMSs have superior mechanical properties. To investigate the mechanical properties of the developed TPMS-based AC, we fabricated another sample using the thermoplastic polyurethane (TPU) material and conducted a compression test. Note that, for the consideration of cost, the unit cell size is set as 2.5 cm for this sample. Fig. 4a shows a schematic of the compression test. We conducted ten-rounds of compression and present the stress (σ)–strain (ε) curves of the first, fourth, seventh and tenth rounds, as well as the simulation results [see section 4 of the Supplementary Material for details] in Fig. 4b, from which we can observe that the stress–strain curves of both compression and release processes for these rounds are almost the same, demonstrating the recoverability of the TPMS-based AC made of TPU. Meanwhile, Fig. 4c–e illustrate the initial structure, the deformed structure under the maximum applied force, and the recovered structure after the external force is removed, respectively. It can be observed that the unit cell undergoes significant deformation when the external force is exerted and then recovers to the initial state

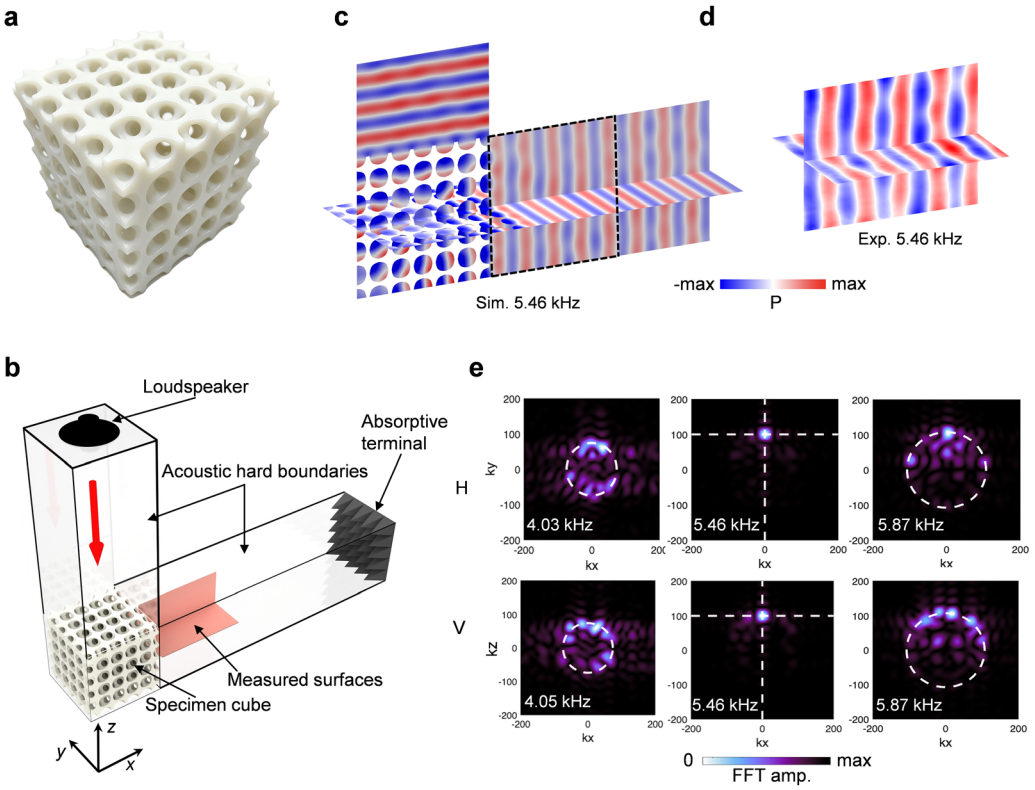

Fig. 2 The experimental validation of the property of a 3D acoustic void space of the TPMS-based AC. (a) The 3D-fabricated TPMS-based AC. (b) A schematic of the experimental setup. (c) The simulation result of the wave impinging normally on the TPMS-based AC along the negative *z* direction and turning into positive in the *x* direction. (d) The experimentally measured field of domain denoted by the dashed box in (c). (e) The FFT of the acoustic pressure fields measured within the horizontal (upper panel) and vertical (bottom panel) planes.

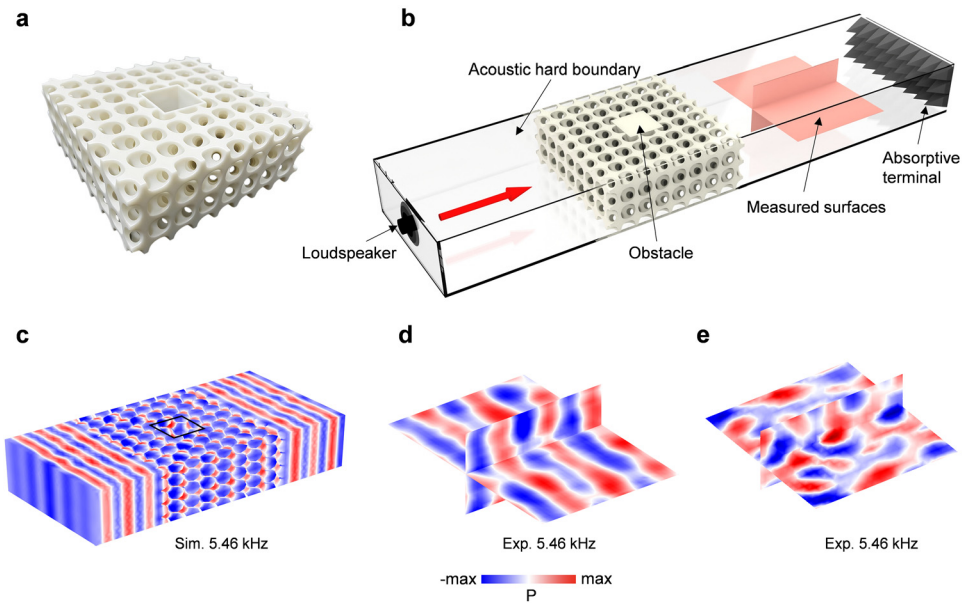

Fig. 3 The experimental validation of the cloaking property of the TPMS-based AC. (a) The 3D-fabricated TPMS-based AC with 2 × 2 × 3 unit cells removed. (b) The schematic of the experimental setup. (c) The simulated acoustic pressure field at the frequency of the Dirac-like point. (d) The experimentally measured field. (e) The experimentally measured field after the TPMS-based AC is removed.

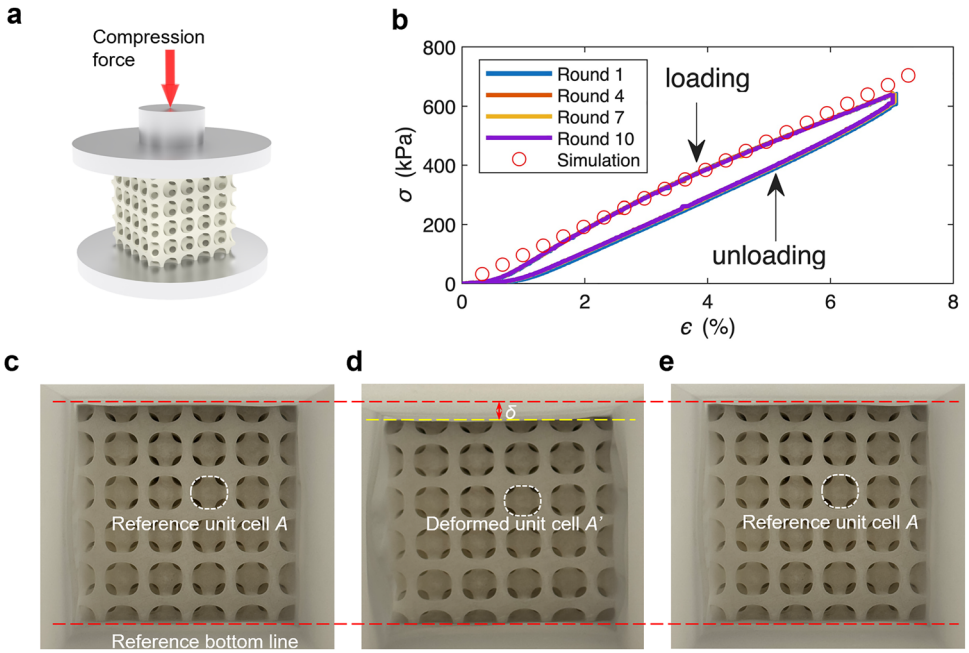

Fig. 4 The mechanical properties of the TPMS-based AC made of TPU. (a) A schematic of the experimental setup. (b) The stress (σ)–strain (ε) curves of multi-round compressions, where the circles denote the simulation results. (c) The TPMS-based AC of the initial state. (d) The deformed TPMS-based AC under the maximum applied force. (e) The recovered structure after the external force is removed.

after the force is removed. This property can be used for designing an acoustic switch.[11]

3. Conclusion

In conclusion, we propose a TPMS-based AC exhibiting an accidentally degenerated Dirac-like cone, at the frequency of which the normalized effective mass density and effective compressibility become zero simultaneously. Empowered by such a double-zero index, the tunneling of acoustic waves in 3D space is experimentally demonstrated. Due to the advantage of the better integration with structural components, the acoustic cloaking effects, which have not been achieved using previous 3D double-zero index structures, are also numerically and experimentally demonstrated. Furthermore, the superior mechanical properties of the TPMS-based AC made of TPU are analyzed, which can be used for designing switchable acoustic devices. The TPMS-based AC as a fully connected solid material provides a route for creating fabrication-friendly double-zero index acoustic structures that can be reconfigured towards various practical application scenarios, such as cloaking, focusing and wavefront shaping. Compared with previous double-zero index ACs that almost cannot withstand external loads (if extra support structures are not introduced) due to the disconnected solid material, the TPMS-based AC possesses load bearing capacity. Meanwhile, the unique geometrical characteristics endow the acoustic structure with lightweight and superior mechanical properties, making it favorable for developing multifunctional integrated acoustic devices.

4. Experimental section

The samples in Fig. 2a and 3a were fabricated using 3D printing with photosensitive resin, whereas that in Fig. 4 was printed using TPU. For the acoustic tests, we used a Sound and Vibration Module (PXIe-4464) to generate a chirp signal to the power amplifier (BSWA, PA50), thereby driving the loudspeaker (Peerless, 3.5″ Woofer) to produce the sound source. A $\frac{1}{4}$-inch microphone mounted on a mobile displacement platform was used to capture the acoustic pressure field, and the signal was amplified by a signal conditioner (BK1704) before being acquired by the module (PXIe-4464). Data processing, including FFT, was conducted on a host PC using LabVIEW, which interfaced with the Sound and Vibration Module. In the compression test, a cubic specimen with a unit cell size of 2.5 cm and a $5 \times 5 \times 5$ array was fabricated using TPU. A universal testing machine (Haida, HD-F750A) was used to apply the compressive load. The specimen was positioned at the center of a flat structural steel plate fixture. The compression force was gradually applied to the top surface of the specimen from 0 to 10 kN, then gradually released to complete one testing cycle.

Conflicts of interest

The authors declare no conflict of interest.

Data availability

The data that support the findings of this study are available from the corresponding author upon reasonable request.

Supplementary information (SI) is available. See DOI: https://doi.org/10.1039/d6mh00635c.

Acknowledgements

This work was supported by the National Natural Science Foundation of China (No. 92263208, 12304494, and 12102134), National Key R&D Program of China (Grants No. 2022YFA1404400 and No. 2022YFA1404403), the Fundamental Research Funds for the Central Universities, the Research Grants Council of Hong Kong SAR (No. 15214323, 15200922, 15202820, and AoE/P-502/20), and Hong Kong Innovation and Technology Commission *via* project ''Smart Railway Technology and Applications'' (No. K-BBY1).

References

1 L. Han and S. Che, *Adv. Mater.*, 2018, **30**, 1705708.
2 Y. Guo, M. I. Rosa and M. Ruzzene, *Adv. Sci.*, 2023, **10**, 2205723.
3 L. C. Felix, R. Ambekar, R. M. Tromer, C. F. Woellner, V. Rodrigues, P. M. Ajayan, C. S. Tiwary and D. S. Galvao, *Small*, 2024, **21**, 2400351.
4 C. J. Ejeh, I. Barsoum and R. K. A. Al-Rub, *Mater. Des.*, 2025, **253**, 113959.
5 Y. Guo, M. I. N. Rosa, M. Gupta, B. E. Dolan, B. Fields, L. Valdevit and M. Ruzzene, *Adv. Funct. Mater.*, 2022, **32**, 2204122.
6 T. Silva, J.-Y. Lu, R. K. Abu Al-Rub and D.-W. Lee, *Int. J. Mech. Mater. Des.*, 2023, **20**, 317.
7 H. Dai, H. Xiao, Z. Qiu, N. Dai and L. Zhou, *Adv. Eng. Mater.*, 2024, **26**, 2400017.
8 Q. An, D. Li, W. Liao, T. Liu, Z. Qu, G. Wang and X. Li, *Adv. Funct. Mater.*, 2025, **35**, 2414629.
9 N. B. Cáceres, *Elastic wave propagation in cubic lattices with triply periodic minimal surfaces*, MS thesis, Wichita State University, 2019.
10 T. Gao, K. Liu, X. Wang, L. Shen, Y. Zhao, K. Wei and Z. Wang, *Compos. Commun.*, 2023, **44**, 101745.
11 P. Xue, H. Dai and L. Zhou, *Adv. Eng. Mater.*, 2023, **25**, 2201144.
12 Z. Li, X. Wang, Z. Wang, X. Li, X. Yu, S. Ramakrishna, Y. Lu and L. Cheng, *Mater. Today*, 2025, **89**, 151–171.
13 D. Lee, B. Oh, J. Park, S.-W. Moon, K. Shin, S.-M. Kim and J. Rho, *Nat. Commun.*, 2024, **15**, 3044.
14 B. Oh, K. Kim, D. Lee and J. Rho, *Mater. Today Phys.*, 2023, **39**, 101273.
15 Y. Jang, B. Oh, E. Kim and J. Rho, Bidirectional Asymmetric Frequency Conversion in Nonlinear Phononic Crystals, *Phys. Rev. Lett.*, 2025, **135**, 036603.
16 F. Ma, C. Wang, Y. Du, Z. Zhu and J. H. Wu, *Mater. Horiz.*, 2023, **9**, 653–662.
17 L. Fan, Z. Lan, Y. Chen, J. Zhu and Z. Su, *Mater. Horiz.*, 2025, **12**, 6334–6341.
18 X. Wang, Z. Liang, Z. Tang, S. Rui, K. Li and F. Ma, *Mater. Horiz.*, 2025, **12**, 4289–4303.
19 X. Li, J. W. Chua, X. Yu, Z. Li, M. Zhao, Z. Wang and W. Zhai, *Adv. Sci.*, 2023, **11**, 2305232.
20 X. Huang, Y. Lai, Z. H. Hang, H. Zheng and C. T. Chan, *Nat. Mater.*, 2011, **10**, 582.
21 I. Liberal and N. Engheta, *Nat. Photonics*, 2017, **11**, 149.
22 P. Moitra, Y. Yang, Z. Anderson, I. I. Kravchenko, D. P. Briggs and J. Valentine, *Nat. Photonics*, 2013, **7**, 791.
23 Y. Chen, F. Meng, G. Li and X. Huang, *Acta Mater.*, 2019, **164**, 377.
24 C. Xu and Y. Lai, *Phys. Rev. B*, 2017, **95**, 045124.
25 C. Xu, M. Farhat and Y. Wu, *Appl. Phys. Lett.*, 2021, **119**, 224102.
26 H. Chu, Y. Zhang, J. Luo, C. Xu, X. Xiong, R. Peng, M. Wang and Y. Lai, *Opt. Express*, 2021, **29**, 18070.
27 C. Xu, K. Lyu and Y. Wu, *Europhys. Lett.*, 2023, **141**, 15002.
28 D. Yan, A. S. Shalin, Y. Wang, Y. Lai, Y. Xu, Z. H. Hang, F. Cao, L. Gao and J. Luo, *Phys. Rev. Lett.*, 2025, **134**, 243802.
29 N. Kinsey, C. DeVault, A. Boltasseva and V. M. Shalaev, *Nat. Rev. Mater.*, 2019, **4**, 742.
30 Z. Lin, L. Christakis, Y. Li, E. Mazur, A. W. Rodriguez and M. Lončar, *Phys. Rev. B*, 2018, **97**, 081408.
31 C. Xu, H. Chu, J. Luo, Z. H. Hang, Y. Wu and Y. Lai, *Phys. Rev. Lett.*, 2021, **127**, 123902.
32 N. Mattiucci, M. J. Bloemer and G. D'Aguanno, *Opt. Express*, 2014, **22**, 6381.
33 J. Mei, Y. Wu, C. T. Chan and Z.-Q. Zhang, *Phys. Rev. B: Condens. Matter Mater. Phys.*, 2012, **86**, 035141.
34 C. Xu, S. Huang, Z. Guo, H. Jiang, Y. Li, Y. Wu and H. Chen, *Phys. Rev. Appl.*, 2022, **17**, 054025.
35 M. Dubois, C. Shi, X. Zhu, Y. Wang and X. Zhang, *Nat. Commun.*, 2017, **8**, 14871.
36 C. Xu, G. Ma, Z.-G. Chen, J. Luo, J. Shi, Y. Lai and Y. Wu, *Phys. Rev. Lett.*, 2020, **124**, 074501.
37 C. Xu, J. Shi, X. Liu, Z.-G. Chen, Y. Wu and Y. Lai, *Phys. Rev. Lett.*, 2025, **135**, 046902.
38 A. Jones, M. Leary, S. Bateman and M. Easton, *Softw. Impacts*, 2021, **10**, 100167.

